Research Article

Nano Research
2019, 12(9): 2296–2301

ISSN 1998-0124 CN 11-5974/O4
https://doi.org/10.1007/s12274-019-2409-5

Room-temperature ligancy engineering of perovskite electrocatalyst for enhanced electrochemical water oxidation

Junchi Wu[1,§], Yuqiao Guo[1,§], Haifeng Liu[3], Jiyin Zhao[1], Haodong Zhou[1], Wangsheng Chu[2], and Changzheng Wu[1] (✉)

[1] *Hefei National Laboratory for Physical Sciences at the Microscale, Collaborative Innovation Center of Chemistry for Energy Materials (iChEM), and CAS Key Laboratory of Mechanical Behavior and Design of Materials, University of Science and Technology of China, Hefei 230026, China*
[2] *National Synchrotron Radiation Laboratory, University of Science and Technology of China, Hefei 230026, China*
[3] *Analytical and Testing Center, Southwest University of Science and Technology, Mianyang 621010, China*
[§] *Junchi Wu and Yuqiao Guo contributed equally to this work.*

Received: 29 January 2019 / **Revised:** 20 March 2019 / **Accepted:** 8 April 2019

ABSTRACT

Perovskite oxides are significant candidates to develop electrochemical catalysts for water oxidation in consideration of their high catalysis capacity, low costing and excellent stability. Rational design of coordination structure and overcoming poor electronic transport are regarded as critical factors for outstanding perovskite-based oxygen evolution reaction (OER) catalysts. Herein, we report a mild chemical oxidation method to realize ligancy engineering from strongly-correlated brownmillerite $Sr_2Co_2O_5$ to perovskite phase $Sr_2Co_2O_{5.5}$, along with abundant oxygen vacancies formation and greatly boosted electric conductivity, which helps to form the active species of Co hydroxide/oxide on the surface of catalysts. The coupling effect of catalytic kinetics and unimpeded electronic movement brings high OER activities in $Sr_2Co_2O_{5.5}$ with a low onset potential and a small Tafel slope. Our work not only displays in-depth understanding into the relationship among catalysis performance and multiple physical degrees of freedom, but also paves a new path to develop high-efficient electrochemical catalysts.

KEYWORDS

perovskite oxides, ligancy engineering, oxygen evolution reaction, electrocatalysts

1 Introduction

The development of high-efficient, inexpensive, and stable electrocatalysts for the oxygen evolution reaction (OER) is critical for many electrochemical energy conversion technologies, such as metal-air batteries, water splitting, and regenerative fuel cells [1–4]. Up to now, benchmarks of OER catalysts are expensive and scarce novel metal oxides, such as IrO_2 and RuO_2, which hinders their extensive applications [5, 6]. Perovskite oxides, which are made up of alkaline earth cations (A-site), transition metal cations (B-site) and oxygen anions, have shown attractive physical properties and impressive catalytic potential in oxidation reaction [7–9]. Therefore they are considered as low-cost alternative of precious-metal-based materials [10–12]. Expect for outstanding OER activity and stability, perovskite with common BO_6 octahedrons as basic structural units and variable-valence B-site transition metal cations as catalytic active sites provides an ideal platform to design high-performance catalysts and understand OER catalysis mechanism. In previous studies, OER process was considered to be multiple-step reaction process, including realization of fast reactive molecule absorption, intermediate atom transfer and product molecule dissociation, which is tightly associated with strength of B–O bonds [13–15] and coordination structure around B-site atoms [16–18]. Based on the theory, various strategies were designed to modulate B–O bonding or create unsaturated coordination environment of B-site atoms. For example, vibronic super-exchange interaction was designed to weaken B–O bonding via strongly asymmetric ligand field effect and largely optimized the OER performance of La_2NiMnO_6 [19]; ordered oxygen vacancies and abundant unsaturated BO_5 pyramids have been found to be responsible for high-efficient OER properties in $CaMnO_{3-x}$ and $RE_{0.5}Ba_{0.5}Co_2O_{5+x}$ [20, 21]. Up to data, the main-stream coordination modulation methods are limited in deoxygenation at high temperature or A-site doping by high-valence rare earth atoms. Nevertheless, structure damage is inevitable when reduction in a high-temperature step or replacement with exotic atoms, which not only affects electron transferring across catalyst particles, but also makes catalysis mechanism complicated and confusing [22]. Thus, it is urgent to find straightforward methods for mild coordination modulation in perovskite-type transition metal oxides to realize the enhanced electrochemical catalysis performance.

Brownmillerite phase (BM phase) $Sr_2Co_2O_5$ is one kind of layered perovskite-type oxides and has been found to be an efficient OER catalyst in alkaline solution due to alterable Co valent state and reversible surface redox reaction [23, 24]. However, the essence of oxygen-vacancies-free brownmillerite superlattice structure contains only one half of catalytically active MO_6 octahedron while another half of catalytically inactive MO_4 tetrahedron. Even worse, brownmillerite $Sr_2Co_2O_5$ displays insulator-like electric transport property on account of strong antiferromagnetism (AFM) correlative charge order coming from alternant CoO_6 octahedron and CoO_4 tetrahedron [25]. Thus the coordination form of Co–O in $Sr_2Co_2O_5$ hinders itself to own better electrochemical performance to a great extent.

Herein, we used a simple one-step chemical oxidation with NaClO aqueous solution to realize ligancy modulation of BM phase $Sr_2Co_2O_5$, successfully transformed CoO_4 tetrahedrons to CoO_5 pyramids and greatly enhanced the OER performance of $Sr_2Co_2O_5$. As Fig. 1 shown,

Address correspondence to czwu@ustc.edu.cn

oxygen anions would intercalate into the $Sr_2Co_2O_5$ superlattice and switch $Sr_2Co_2O_5$ to perovskite phase $Sr_2Co_2O_{5+x}$ via a cascade of distorted CoO_4 layer to produce ordered CoO_5 pyramids. Oxygen ions can smoothly transfer through exchange between CoO_5 pyramid and adjacent CoO_6 octahedrons. At the same time, antiferromagnetic Mott insulator $Sr_2Co_2O_5$ converts to ferromagnetic $Sr_2Co_2O_{5.5}$ with high electric conductivity. Electrochemical OER performance has been greatly promoted in $Sr_2Co_2O_{5.5}$ via ligancy modulation. This work provides a new sight into designing high-performance perovskite oxide based OER catalysts.

2 Experimental

2.1 Chemicals

Cobalt(II) nitrate hexahydrate (99.99%), strontium nitrate (99.97%), citric acid monohydrate (≥ 98%), ethylene glycol (AR), barium nitrate (≥ 99.5%), iron nitrate nonahydrate (≥ 98.5%) and potassium hydroxide (AR) were purchased from Sinopharm Chemical Reagent Co. Ltd. All chemicals were used without further purification.

2.2 Experiment

Brownmillerite-phase $Sr_2Co_2O_5$ powder and perovskite $Ba_{0.5}Sr_{0.5}Co_{0.8}Fe_{0.2}O_{3-\delta}$ (BSCF) powder were synthesized by conventional sol-gel technique. In detail, quantitative nitrates were dissolved in 80 mL citric acid concentrated aqueous solution containing 60 mmol citric acid under stirring at 80 °C. Then 3 mL ethylene glycol was added and stirred for another hour at 80 °C. The solution was dried at 120 °C to get an organic resin. The so-formed organic resin was further dried at 200 °C overnight and then annealed at 500 °C for 12 h to get a black predecessor powder. Predecessor was heated at 800 °C for 10 h in air to obtain hexagonal $Sr_2Co_2O_5$ powder and perovskite $Ba_{0.5}Sr_{0.5}Co_{0.8}Fe_{0.2}O_{3-\delta}$ powder. The brownmillerite-type $Sr_2Co_2O_5$ was obtained by quenching hexagonal $Sr_2Co_2O_5$ phase from 1,000 °C to liquid N_2 temperature. Deficient-perovskite-type $Sr_2Co_2O_{5.5}$ powder was obtained by immersing $Sr_2Co_2O_5$ into NaClO solution at room temperature. All product was carefully washed with water and alcohol for several times and dried in vacuum overnight before further characterization and electrochemical tests.

2.3 Characterization

X-ray powder diffraction (XRD) was performed using a Philips X'Pert Pro Super diffractometer with Cu-Kα radiation (λ = 1.54178 Å). The field-emission scanning electron microscopy (FE-SEM) images were taken on a JEOL JSM-6700F SEM. The high-resolution transmission electron microscopy (HRTEM) images and energy dispersive X-ray spectra (EDS) were obtained on a JEM 2100F (field-emission) transmission electron microscope equipped with an Oxford INCA x-sight EDS Si(Li) detector: The microscope was operated at an acceleration voltage of 200 kV. X-ray photoelectron spectroscopy (XPS) was measured on ESCALAB MK II X-rayphotoelectron spectrometer equipped with an Mg-Kα excitation source. The absorption spectra of Co K-edge were collected in transmission mode using a Si (111) double-crystal monochromator at the X-ray absorption fine structure (XAFS) station of the beamline 14W1 of the Shanghai Synchrotron Radiation Laboratory (SSRL, Shanghai) at room temperature. Electrical conductivity measurements were carried out on pressed pellets using standard four probe transport measurement on commercial apparatus of Physical Property Measurement System (PPMS, Quantum Design). Magnetism was measured using magnetometry on a superconducting quantum interference device magnetometer (SQUID).

2.4 Electrochemical test

Electrochemical measurements were performed in a three-electrode system on an electrochemical workstation (CHI760E) by using an Ag/AgCl (3.3 M KCl) electrode as the reference electrode, Pt electrode as the counter electrode, and a Pine Bipotentiostat rotating disk electrode (RDE) with one of the catalysts as the working electrodes. In a typical procedure, 4 mg of samples and 40 μL of Nafion solution (5 wt.%, Sigma Aldrich) were dispersed in 1 mL of water-isopropanol solution (volume ratio of 3:1), and then the aforementioned solution was sonicated for 30 min. After that, 15 μL of the as-prepared homogeneous ink was loaded onto an RDE. Linear-sweep voltammetry was conducted at a scan rate of 5 mV/s in 0.1 M KOH solution (purged with oxygen for 30 min). Alternating current (AC) impedance measurements of the catalysts were performed in the same configuration at the potential of 0.7 V vs. Ag/AgCl from 100 kHz to 100 mHz with a Zahner IM6 electrochemical workstation in O_2-saturated 0.1 M KOH.

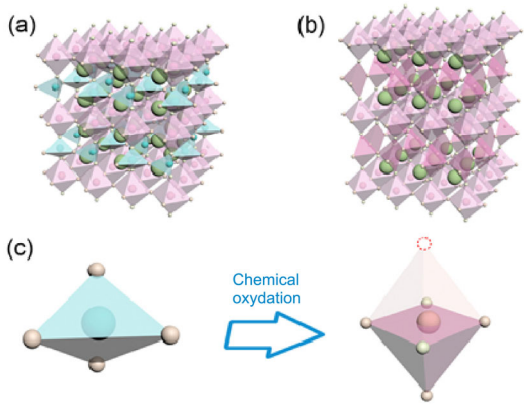

Figure 1 Crystal structures of (a) brownmillerite $Sr_2Co_2O_5$ and (b) perovskite $Sr_2Co_2O_{5.5}$. (c) Illustration of CoO_4 tetrahedron transforming to CoO_5 pyramid.

3 Results and discussion

As shown in Fig. 2(a), we synthesized high-quality BM phase $Sr_2Co_2O_5$ with three peaks near 33° due to a quasi-two-dimensional feature of BM structure. The bright and focused selected-area electron diffraction pattern in Fig. S1(a) in the Electronic Supplementary Material (ESM) implies perfect crystalline quality. After mild room-temperature oxidation treatment, BM-phase transforms to a new phase with degenerative XRD peak, implying the elevation of crystalline symmetry to cubic lattice. The lattice parameter of the new phase equals 0.34 nm, which corresponding to $Sr_2Co_2O_{5.5}$ in previous research [26]. The structural conversion is further confirmed by HRTEM tests. Figure 2(b) shows a tetragonal lattice symmetry with two lattice fringes of 0.79 and 0.28 nm, corresponding to (020) and (002) with 90° included angle, which are well matched with BM-phase $Sr_2Co_2O_5$. After oxidation, lattice fringes with the distance of 0.27 nm and a 60° included angle are indexed to {110} lattice plane of perovskite phase $Sr_2Co_2O_{5.5}$. Meanwhile, selected area electron diffraction (SAED) image with hexagonal bright lattice matches well with cubic $Sr_2Co_2O_{5.5}$ along [111] direction. Meanwhile, the size and morphology of $Sr_2Co_2O_{5.5}$ are not changed after the mild oxidation process, as present in SEM images in Fig. S2 in the ESM. The structural analysis visually demonstrates the successful structural transformation during the oxidation process.

Furthermore, XAFS spectrum was obtained to survey the local symmetry evolution around Co atoms. As seen in Fig. 2(d), the distinct blue-shifted X-ray absorption near edge structure (XANES) edge by 1.5 eV after oxidation implies the increased average valence of Co atoms after structural transition. XPS study was carried out to provide detail ratio of Co^{3+} and Co^{4+} in $Sr_2Co_2O_{5.5}$. As shown in Fig. S3 in the ESM, Co 2p XPS spectrum can be fitted with two sets of XPS peaks with similar integral area, suggesting nearly equal Co^{3+} and Co^{4+} components and an average covalence state of +3.5

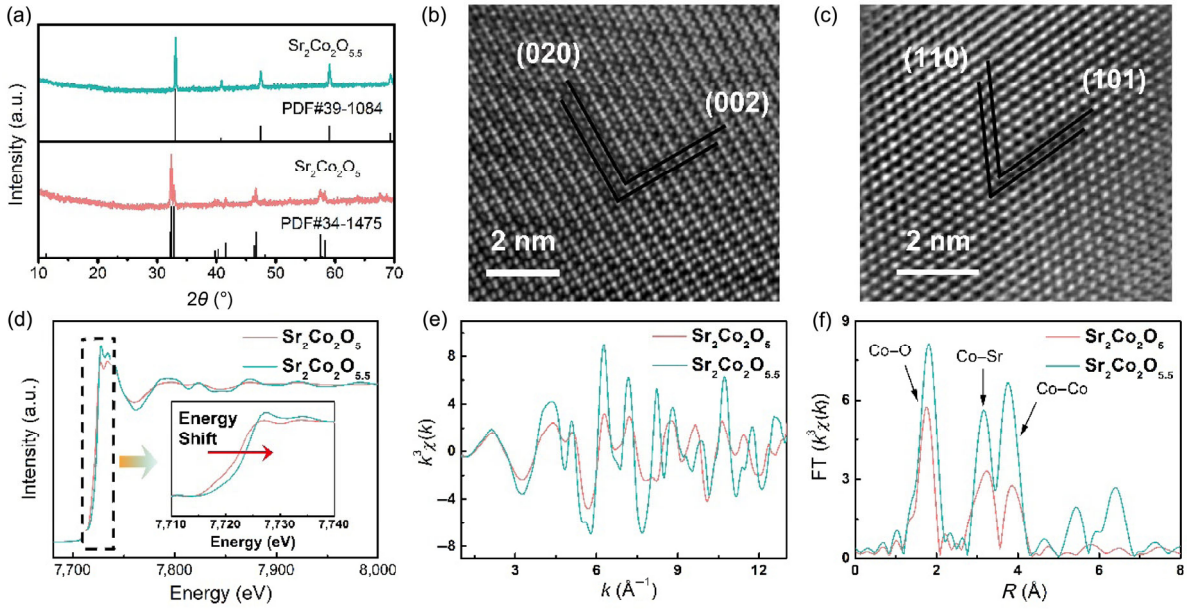

Figure 2 (a) XRD of the $Sr_2Co_2O_5$ and $Sr_2Co_2O_{5.5}$. HRTEM images of (b) $Sr_2Co_2O_5$ and (c) $Sr_2Co_2O_{5.5}$. Co *K*-edge (d) XAFS spectra, (e) EXAFS oscillation function $k^3\chi(k)$ and (f) the corresponding Fourier transformations FT($k^3\chi(k)$) for $Sr_2Co_2O_5$ and $Sr_2Co_2O_{5.5}$; inset of (d): comparison of XANES spectra for $Sr_2Co_2O_5$ and $Sr_2Co_2O_{5.5}$.

in $Sr_2Co_2O_{5.5}$. Besides, an increased Co–O coordination number is suggested by intensifying intensity of white-line peak, boosting amplitude in oscillation function $k^3\chi(k)$ and enhancing intensity in corresponding Fourier transforms FT($k^3\chi(k)$) in $Sr_2Co_2O_{5.5}$ (as shown in Figs. 2(e) and 2(f)). In detail, the increased amplitude in oscillation function $k^3\chi(k)$ shows an increment of scattering path degeneracy due to higher symmetry with advanced degree of order and coordination number. Moreover, the FT($k^3\chi(k)$) spectrum exhibits an enhancement of the first coordination shell (Co–O shell) in $Sr_2Co_2O_{5.5}$, supporting the increased Co–O coordination number [27]. In addition, a slightly shift from 1.75 to 1.80 Å hints a prolonged Co–O distance as all tetrahedral CoO_4 geometry with short Co–O distance disappeared. The second peak and the third peak with increased absolute intensity represent the distance of Co–Sr and Co–Co, respectively. It is interesting that the relative intensity reverses after oxidation. This increased absolute intensity is caused by ordering of Co in a more symmetric environment and the intensity of Co–Co shell gains more than Co–Sr shell. To further check the local environment of Co–O polyhedron, pre-edge peaks in XAFS are meticulously analyzed since it has strong finger-print effect to symmetry environment and geometry coordination environment of central atoms. The pre-edge feature in our results accords with the dipole-forbidden transition from 1s to 3d, which is forbidden by O_h symmetry in octahedral CoO_6 [28]. A blue-shift is also found, further testifying the raised covalent state. More importantly, even though the pre-shift peak gets slightly broader, its intensity remains almost unchanged, verified incomplete oxidation from CoO_4 tetrahedron to CoO_5 pyramids. The abundant CoO_5 pyramids with Co–O unsaturated coordination provide ample oxygen vacancies homogeneously spread over the cubic lattice, which prompts $Sr_2Co_2O_{5.5}$ to own high potential for electrochemical water splitting.

As a typical strong electronic correlation system, along with dramatic structural phase transition, the intrinsic physical properties of $Sr_2Co_2O_{5.5}$ have changed drastically, especially spin-arrangement dependent magnetism and electric transport. We measured the temperature dependent susceptibility curves (*M*–*T*) of $Sr_2Co_2O_5$ and $Sr_2Co_2O_{5.5}$ from 10 to 300 K at 500 Oe, as shown in Fig. 3(a). Negligible susceptibility within our test region implies the possible antiferromagnetic ground state of $Sr_2Co_2O_5$. However, no AFM phase transition is observed within the region due to its high Neel temperature (about 570 K in previous report [29]). A linear field-dependent magnetization curve (*M*–*H*) at room-temperature for $Sr_2Co_2O_5$ (as shown in Fig. 3(b)) gives further evidence for the AFM exchange coupling between neighboring Co in $Sr_2Co_2O_5$. As many AFM materials, such as $LaMnO_3$ and La_2CuO_4, strong electronic correlation blocks electrons from moving freely across the metal-oxygen-metal pathways and makes them to be Mott-type insulator [30, 31]. An insulating electric transport in $Sr_2Co_2O_5$ is observed with a large room-temperature resistivity of 8,000 Ω·cm, which is an obstacle for electrochemical catalysis. Unlike the AFM ground state in $Sr_2Co_2O_5$, we find $Sr_2Co_2O_{5.5}$ displays paramagnetism near room temperature and ferromagnetism (FM) below 160 K, which obviously elucidates spin rearrangement after successful oxidation. Curie–Weiss law is utilized to analysis spin arrangement in $Sr_2Co_2O_{5.5}$ with the paramagnetic data in the inverse susceptibility ($1/\chi$) plot (shown in Fig. S4 in the ESM). A positive Weiss constant at 160 K is obtained, indicating a strong FM coupling between adjacent Co atoms. The efficient magnetic moment μ_{eff}, which stands for the numbers of unpaired electrons in a formula unit, can be calculated to be 2.9 μ_B for every $Sr_2Co_2O_{5.5}$ formula. An S-shaped *M*–*H* curve with a saturation magnetization of about 43.5 emu/g for $Sr_2Co_2O_{5.5}$ at 10 K is another evidence for the FM interaction between adjacent Co–Co. Considering the parallel arrangement of all unpaired electrons in the saturation region, the number of unpaired electrons for each Co can be predicted via constructing a bridge connecting microscopic atomic magnetic moment and macroscopic saturated magnetic moment. The predicted number of unpaired electron is 2.96 for every $Sr_2Co_2O_{5.5}$ formula, which agrees well with the value obtained from Curie–Weiss law. The rational filling state of 3d electrons can be deduced to be 50% Co^{3+} in intermedium spin state (IS) and 50% Co^{4+} in low spin state (LS). Notable, IS Co^{3+} with $t_{2g}^5e_g^1$ occupancy state is regarded to own optimal binding energy of oxygen-related intermediate species and therefor can powerfully promote its OER activity [32]. On account of the magnetic transition, electronic transport in $Sr_2Co_2O_{5.5}$ is much easier with a small room-temperature electric resistivity of only 0.7 Ω·cm, 10,000 times less than $Sr_2Co_2O_5$. Comprehension based on double-exchange mechanism is illustrated in Fig. 3(d), which has been widely applied to explain the relationship between magnetism and electric transport

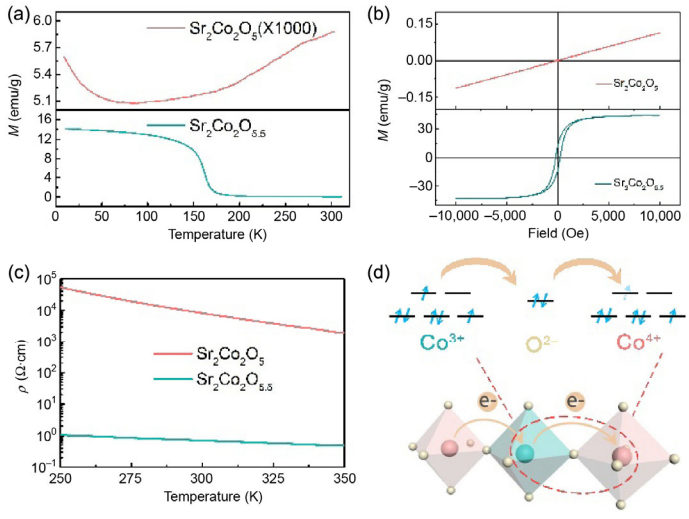

Figure 3 (a) Susceptibility curves at 500 Oe and (b) magnetization curves at 300 K of $Sr_2Co_2O_5$ and at 10 K of $Sr_2Co_2O_{5.5}$. (c) Temperature-dependence resistivity of $Sr_2Co_2O_5$ and $Sr_2Co_2O_{5.5}$ from 250 to 350 K. (d) Scheme of spin regulation in $Sr_2Co_2O_{5.5}$ and double-exchange mechanism of Co^{3+}–O–Co^{4+}.

in perovskites [33, 34]. The combination of electronic configuration optimization and enhanced electronic transport promotes $Sr_2Co_2O_{5.5}$ to be an effective OER catalyst.

The OER performance of $Sr_2Co_2O_5$ and $Sr_2Co_2O_{5.5}$ was tested in a standard three-electrode system with oxygen-saturated 0.1 M KOH aqueous solution as electrolyte. To further confirm the performance of our samples, one of the best perovskite OER catalysts, BSCF, was synthesized and utilized as a reference [35]. To highlight the intrinsic electrochemical catalysis performance, additive (e.g. acetylene black) was not used in any of our tests. Linear-scan voltammetry (LSV) was adopted for determining OER performance and *iR*-correction was utilized to eliminate potential error derived from solution resistance. The *iR*-corrected LSV results for all samples are shown in Fig. 4(a). $Sr_2Co_2O_{5.5}$ exhibits an onset potential of 1.50 V vs. RHE, which is similar to 1.49 V of BSCF and much lower than 1.54 V of $Sr_2Co_2O_5$. The current density reaches 1 mA/cm^2 at an overpotential η of 347.3, 406.3 and 401.0 mV for $Sr_2Co_2O_{5.5}$, $Sr_2Co_2O_5$ and BSCF, respectively (Fig. S6 in the ESM). Figure 4(b) plots current density at special potentials. Outstanding performance of $Sr_2Co_2O_{5.5}$ can be distinguished: 1.6 times, 5.1 times and 7.7 times enhanced current density than $Sr_2Co_2O_5$ at 1.60, 1.65 and 1.70 V, respectively. Tafel slopes are plotted in Fig. 4(c) as significant performance criterion and to explore inner mechanism of the electrochemical pathway. As shown in Fig. 4(d), $Sr_2Co_2O_{5.5}$ displays a much lower Tafel slope of 47 mV/dec than BSCF of 99 mV/dec and $Sr_2Co_2O_5$ of 61 mV/dec, which further highlighted the remarkable OER performance of $Sr_2Co_2O_{5.5}$. The OER performance of $Sr_2Co_2O_{5.5}$ is also comparable to the most reported OER catalysts as listed in Table S1 in the ESM. The much lower Tafel slope implies the determining step change from –OH absorption to O–OH formation, profiting from vast absorption sites providing luxuriant oxygen defects in $Sr_2Co_2O_{5.5}$ [36]. Besides, electrochemical impedance spectroscopy (EIS), as displayed in Fig. 4(d), was conducted to comprehend actual reaction kinetics. The equivalent circuit shown by Nyquist plots can be fitted to assembly of a solution resistance (R_s), a constant phase element (CPE), and a charge transfer resistance (R_{ct}). All catalysts were tested in the same condition with similar R_s of about 40 Ω. Compared with $Sr_2Co_2O_5$, $Sr_2Co_2O_{5.5}$ reveals a dramatic reduced interfacial charge transfer resistance of only 30 Ω, indicating an accelerated charge transfer process on the interface between electrolyte and $Sr_2Co_2O_{5.5}$ catalyst. In hence, the advantageous OH absorption in pyramid CoO_5 and fast electron transfer pathway in $Sr_2Co_2O_{5.5}$ is responsible for the reduction of OER barriers [37]. To further verify $Sr_2Co_2O_{5.5}$ to be an outstanding OER catalyst, we also tested the stability at η = 450 mV within 48 h and no obvious performance degradation is observed (shown in Fig. S7 in the ESM). Combined with polarization curves results, Tafel slope analysis and EIS fitting, we highlight the electrochemical OER performance of cubic phase $Sr_2Co_2O_{5.5}$, benefitting from its charge transfer motorway and luxurious surficial active sites.

To in-depth investigation of facilitated OER performance, we compared the HRTEM images of perovskite particles before and after the oxidation process. As shown in Fig. 5(a), $Sr_2Co_2O_5$ obtained from high-temperature synthesis reveals clean surface with high crystalline quality. While $Sr_2Co_2O_{5.5}$ displays crystalline core encapsulated by an apparent amorphous shell layer with a thickness of 4–5 nm, as shown in Fig. 5(b). To confirm the constituent of amorphous shell, the element distribution are imaged via EDS mapping (shown in Fig. S11 in the ESM). A loss of Sr near the surface of $Sr_2Co_2O_{5.5}$ is found, suggesting the formation of amorphous shell is related with dissolution of Sr atoms. XPS Sr 3d spectra are then analyzed in detail to give solid evidence for Sr leaching in alkaline NaClO aqueous. As shown in Figs. 5(c) and 5(d), XPS Sr 3d spectra can be carefully fitted by two sets of XPS peaks, including high-energy surface Sr species and low-energy lattice Sr species [38]. After immersed in alkaline

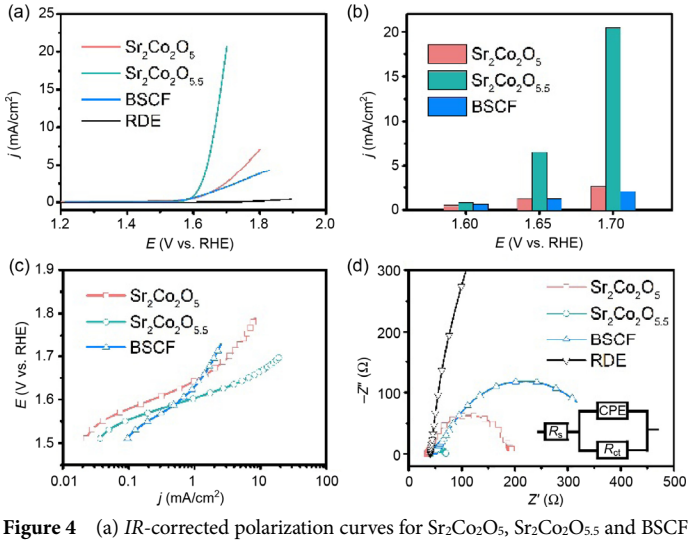

Figure 4 (a) *IR*-corrected polarization curves for $Sr_2Co_2O_5$, $Sr_2Co_2O_{5.5}$ and BSCF in 0.1 M KOH aqueous. (b) Column chart of comparison of current density at 1.60, 1.65 and 1.70 V. (c) Tafel plots for $Sr_2Co_2O_5$, $Sr_2Co_2O_{5.5}$ and BSCF. (d) Electrochemical impedance spectra at 1.665 V with the equivalent circuit (inset).

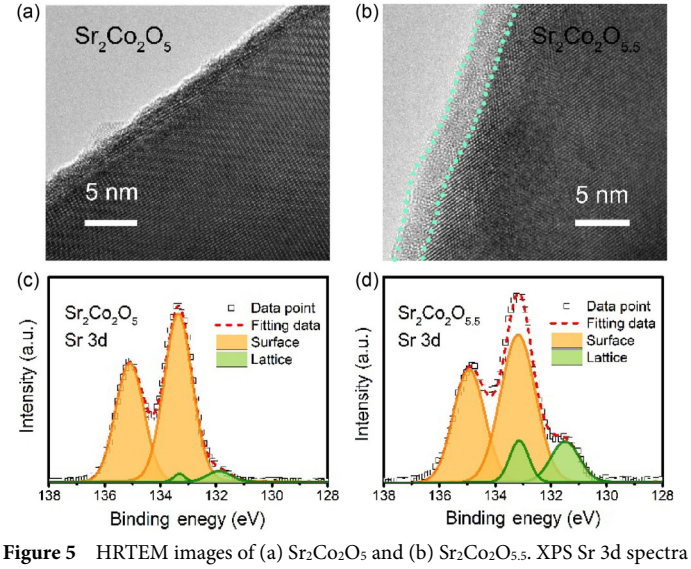

Figure 5 HRTEM images of (a) $Sr_2Co_2O_5$ and (b) $Sr_2Co_2O_{5.5}$. XPS Sr 3d spectra of (c) $Sr_2Co_2O_5$ and (d) $Sr_2Co_2O_{5.5}$.

NaClO aqueous, the intensity of surface Sr species falls markedly, verifying surficial Sr leaching and the formation of amorphous CoO(OH) layer [39]. As mentioned in previous literatures, the amorphous shell made up of CoO(OH) with proper thickness acts as active species in OER process [40–43], which can greatly reinforce electrochemical water oxidation performance on the surface of $Sr_2Co_2O_{5.5}$.

4 Conclusions

In summary, we developed a ligancy engineering in strong-correlated perovskite oxide to synergistically modulate oxygen vacancy concentration, electric transport and e_g electron arrangement by mild oxidation. The coordination structure of CoO_4 tetrahedron in BM phase $Sr_2Co_2O_5$ changes to CoO_5 pyramid in $Sr_2Co_2O_{5.5}$ brings about magnetic ground state changes from antiferromagnetic to ferromagnetic with dramatically boosted conductivity simultaneously. Moreover, alkaline oxidizing agent reconstructs the crystalline surface of catalysts to amorphous CoO(OH) active species, further promoting the OER performance. Combined with outstanding electric transport and active species formation, $Sr_2Co_2O_{5.5}$ displays excellent OER performance with low onset potential and small Tafel slope. We anticipate our work to be newfangled view for raising OER performance of strong-correlated oxides and comprehending the inner mechanism of OER process.

Acknowledgements

This work was financially supported by the National Key R&D Program of Chnia (No. 2017YFA0207301), the National Natural Science Foundation of China (Nos. U1632154, 21890751, 91745113, 11621063, 21601172, and J1030412), National Program for Support of Top-notch Young Professionals, the Fundamental Research Funds for the Central Universities (No. WK2090050043), Youth Innovation Promotion Association of CAS (No. 2018500), Users with Excellence Project of Hefei Science Center (No. CAS2018HSC-UE002). We appreciate the support from the USTC Center for Micro and Nanoscale Research and Fabrication.

Electronic Supplementary Material: Supplementary material (SAED images, SEM images, XPS spectrum, Curie–Weiss fitting, XRD patterns, amperometric *i*–*t* curve, element mapping and performance comparison) is available in the online version of this article at https://doi.org/10.1007/s12274-019-2409-5.

References

[1] Khan, M. A.; Zhao, H. B.; Zou, W. W.; Chen, Z.; Cao, W. J.; Fang, J. H.; Xu, J. Q.; Zhang, L.; Zhang, J. J. Recent progresses in electrocatalysts for water electrolysis. *Electrochem. Energy Rev.* **2018**, *1*, 483–530.

[2] Suen, N. T.; Hung, S. F.; Quan, Q.; Zhang, N.; Xu, Y. J.; Chen, H. M. Electrocatalysis for the oxygen evolution reaction: Recent development and future perspectives. *Chem. Soc. Rev.* **2017**, *46*, 337–365.

[3] Tan, P.; Liu, M. L.; Shao, Z. P.; Ni, M. Recent advances in perovskite oxides as electrode materials for nonaqueous lithium–oxygen batteries. *Adv. Energy Mater.* **2017**, *7*, 1602674.

[4] Song, F.; Bai, L. C.; Moysiadou, A.; Lee, S.; Hu, C.; Liardet, L.; Hu, X. L. Transition metal oxides as electrocatalysts for the oxygen evolution reaction in alkaline solutions: An application-inspired renaissance. *J. Am. Chem. Soc.* **2018**, *140*, 7748–7759.

[5] Seitz, L. C.; Dickens, C. F.; Nishio, K.; Hikita, Y.; Montoya, J.; Doyle, A.; Kirk, C.; Vojvodic, A.; Hwang, H. Y.; Norskov, J. K. et al. A highly active and stable IrO_x/$SrIrO_3$ catalyst for the oxygen evolution reaction. *Science* **2016**, *353*, 1011–1014.

[6] Rana, M.; Mondal, S.; Sahoo, L.; Chatterjee, K.; Karthik, P. E.; Gautam, U. K. Emerging materials in heterogeneous electrocatalysis involving oxygen for energy harvesting. *ACS Appl. Mater. Interfaces* **2018**, *10*, 33737–33767.

[7] Royer, S.; Duprez, D.; Can, F.; Courtois, X.; Batiot-Dupeyrat, C.; Laassiri, S.; Alamdari, H. Perovskites as substitutes of noble metals for heterogeneous catalysis: dream or reality. *Chem. Rev.* **2014**, *114*, 10292–10368.

[8] Hwang, J.; Rao, R. R.; Giordano, L.; Katayama, Y.; Yu, Y.; Shao-Horn, Y. Perovskites in catalysis and electrocatalysis. *Science* **2017**, *358*, 751–756.

[9] Suntivich, J.; Gasteiger, H. A.; Yabuuchi, N.; Nakanishi, H.; Goodenough, J. B.; Shao-Horn, Y. Design principles for oxygen-reduction activity on perovskite oxide catalysts for fuel cells and metal–air batteries. *Nat. Chem.* **2011**, *3*, 546–550.

[10] Han, B. H.; Grimaud, A.; Giordano, L.; Hong, W. T.; Diaz-Morales, O.; Yueh-Lin, L.; Hwang, J.; Charles, N.; Stoerzinger, K. A.; Yang, W. L. et al. Iron-based perovskites for catalyzing oxygen evolution reaction. *J. Phys. Chem. C* **2018**, *122*, 8445–8454.

[11] Mefford, J. T.; Rong, X.; Abakumov, A. M.; Hardin, W. G.; Dai, S.; Kolpak, A. M.; Johnston, K. P.; Stevenson, K. J. Water electrolysis on $La_{1-x}Sr_xCoO_{3-\delta}$ perovskite electrocatalysts. *Nat. Commun.* **2016**, *7*, 11053.

[12] Lee, J. G.; Hwang, J.; Hwang, H. J.; Jeon, O. S.; Jang, J.; Kwon, O.; Lee, Y.; Han, B.; Shul, Y. G. A new family of perovskite catalysts for oxygen-evolution reaction in alkaline media: $BaNiO_3$ and $BaNi_{0.83}O_{2.5}$. *J. Am. Chem. Soc.* **2016**, *138*, 3541–3547.

[13] Malkhandi, S.; Trinh, P.; Manohar, A. K.; Manivannan, A.; Balasubramanian, M.; Prakash, G. K. S.; Narayanan, S. R. Design insights for tuning the electrocatalytic activity of perovskite oxides for the oxygen evolution reaction. *J. Phys. Chem. C* **2015**, *119*, 8004–8013.

[14] Kim, N. I.; Sa, Y. J.; Yoo, T. S.; Choi, S. R.; Afzal, R. A.; Choi, T.; Seo, Y. S.; Lee, K. S.; Hwang, J. Y.; Choi, W. S. et al. Oxygen-deficient triple perovskites as highly active and durable bifunctional electrocatalysts for oxygen electrode reactions. *Sci. Adv.* **2018**, *4*, eaap9360.

[15] Rong, X.; Parolin, J.; Kolpak, A. M. A fundamental relationship between reaction mechanism and stability in metal oxide catalysts for oxygen evolution. *ACS Catal.* **2016**, *6*, 1153–1158.

[16] Wei, C.; Feng, Z. X.; Scherer, G. G.; Barber, J.; Shao-Horn, Y.; Xu, Z. J. Cations in octahedral sites: A descriptor for oxygen electrocatalysis on transition-metal spinels. *Adv. Mater.* **2017**, *29*, 1606800.

[17] Grimaud, A.; Carlton, C. E.; Risch, M.; Hong, W. T.; May, K. J.; Shao-Horn, Y. Oxygen evolution activity and stability of $Ba_6Mn_5O_{16}$, $Sr_4Mn_2CoO_9$, and $Sr_6Co_5O_{15}$: The influence of transition metal coordination. *J. Phys. Chem. C* **2013**, *117*, 25926–25932.

[18] Bothra, N.; Rai, S.; Pati, S. K. Tailoring $Ca_2Mn_2O_5$ based perovskites for improved oxygen evolution reaction. *ACS Appl. Energy Mater.* **2018**, *1*, 6312–6319.

[19] Tong, Y.; Wu, J. C.; Chen, P. Z.; Liu, H. F.; Chu, W. S.; Wu, C. Z.; Xie, Y. Vibronic superexchange in double perovskite electrocatalyst for efficient electrocatalytic oxygen evolution. *J. Am. Chem. Soc.* **2018**, *140*, 11165–11169.

[20] Kim, J.; Yin, X.; Tsao, K. C.; Fang, S. H.; Yang, H. $Ca_2Mn_2O_5$ as oxygen-deficient perovskite electrocatalyst for oxygen evolution reaction. *J. Am. Chem. Soc.* **2014**, *136*, 14646–14649.

[21] Grimaud, A.; May, K. J.; Carlton, C. E.; Lee, Y. L.; Risch, M.; Hong, W. T.; Zhou, J. G.; Shao-Horn, Y. Double perovskites as a family of highly active catalysts for oxygen evolution in alkaline solution. *Nat. Commun.* **2013**, *4*, 2439.

[22] Guo, Y. Q.; Tong, Y.; Chen, P. Z.; Xu, K.; Zhao, J. Y.; Lin, Y.; Chu, W. S.; Peng, Z. M.; Wu, C. Z.; Xie, Y. Engineering the electronic state of a perovskite electrocatalyst for synergistically enhanced oxygen evolution reaction. *Adv. Mater.* **2015**, *27*, 5989–5994.

[23] Takeda, Y.; Kanno, R.; Kondo, T.; Yamamoto, O.; Taguchi, H.; Shimada, M.; Koizumi, M. Properties of $SrMO_{3-\delta}$ (M = Fe, Co) as oxygen electrodes in alkaline solution. *J. Appl. Electrochem.* **1982**, *12*, 275–280.

[24] Jeen, H.; Bi, Z. H.; Choi, W. S.; Chisholm, M. F.; Bridges, C. A.; Paranthaman, M. P.; Lee, H. N. Orienting oxygen vacancies for fast catalytic reaction. *Adv. Mater.* **2013**, *25*, 6459–6463.

[25] Muñoz, A.; de la Calle, C.; Alonso, J. A.; Botta, P. M.; Pardo, V.; Baldomir, D.; Rivas, J. Crystallographic and magnetic structure of $SrCoO_{2.5}$ brownmillerite: Neutron study coupled with band-structure calculations. *Phys. Rev. B* **2008**, *78*, 054404.

[26] Bezdicka, P.; Wattiaux, A.; Grenier, J. C.; Pouchard, M.; Hagenmuller, P. Preparation and characterization of fully stoichiometric $SrCoO_3$ by electrochemical oxidation. *Z. Anorg. Allg. Chem.* **1993**, *619*, 7–12.

[27] Le Toquin, R.; Paulus, W.; Cousson, A.; Prestipino, C.; Lamberti, C. Time-resolved *in situ* studies of oxygen intercalation into $SrCoO_{2.5}$, performed by neutron diffraction and X-ray absorption spectroscopy. *J. Am. Chem. Soc.* **2006**, *128*, 13161–13174.

[28] Piovano, A.; Agostini, G.; Frenkel, A. I.; Bertier, T.; Prestipino, C.; Ceretti, M.; Paulus, W.; Lamberti, C. Time resolved *in situ* XAFS study of the electrochemical oxygen intercalation in $SrFeO_{2.5}$ brownmillerite structure: Comparison with the homologous $SrCoO_{2.5}$ system. *J. Phys. Chem. C* **2011**, *115*, 1311–1322.

[29] Takeda, T.; Yamaguchi, Y.; Watanabe, H. Magnetic structure of $SrCoO_{2.5}$. *J. Phys. Soc. Jpn.* **1972**, *33*, 970–972.

[30] Gao, Y.; Wang, J. J.; Wu, L.; Bao, S. Y.; Yang, S.; Lin, Y. H.; Nan, C. W. Tunable magnetic and electrical behaviors in perovskite oxides by oxygen octahedral tilting. *Sci. China Mater.* **2015**, *58*, 302–312.

[31] Lee, P. A.; Nagaosa, N.; Wen, X. G. Doping a mott insulator: Physics of high-temperature superconductivity. *Rev. Mod. Phys.* **2004**, *78*, 17–85.

[32] Suntivich, J.; May, K. J.; Gasteiger, H. A.; Goodenough, J. B.; Shao-Horn, Y. A perovskite oxide optimized for oxygen evolution catalysis from molecular orbital principles. *Science* **2011**, *334*, 1383–1385.

[33] Peng, X.; Guo, Y. Q.; Yin, Q.; Wu, J. C.; Zhao, J. Y.; Wang, C. M.; Tao, S.; Chu, W. S.; Wu, C. Z.; Xie, Y. Double-exchange effect in two-dimensional MnO_2 nanomaterials. *J. Am. Chem. Soc.* **2017**, *139*, 5242–5248.

[34] De Gennes, P. G. Effects of double exchange in magnetic crystals. *Phys. Rev.* **1960**, *118*, 141–154.

[35] Hong, W. T.; Risch, M.; Stoerzinger, K. A.; Grimaud, A.; Suntivich, J.; Shao-Horn, Y. Toward the rational design of non-precious transition metal oxides for oxygen electrocatalysis. *Energy Environ. Sci.* **2015**, *8*, 1404–1427.

[36] Wang, H. Y.; Hung, S. F.; Chen, H. Y.; Chan, T. S.; Chen, H. M.; Liu, B. In operando identification of geometrical-site-dependent water oxidation activity of spinel Co_3O_4. *J. Am. Chem. Soc.* **2015**, *138*, 36–39.

[37] Riva, M.; Kubicek, M.; Hao, X. F.; Franceschi, G.; Gerhold, S.; Schmid, M.; Hutter, H.; Fleig, J.; Franchini, C.; Yildiz, B. et al. Influence of surface atomic structure demonstrated on oxygen incorporation mechanism at a model perovskite oxide. *Nat. Commun.* **2018**, *9*, 3710.

[38] Cheng, X.; Fabbri, E.; Nachtegaal, M.; Castelli, I. E.; Kazzi, M. E.; Haumont, R.; Marzari, N.; Schmidt, T. J. Oxygen evolution reaction on $La_{1-x}Sr_xCoO_3$ perovskites: A combined experimental and theoretical study of their structural, electronic, and electrochemical properties. *Chem. Mater.* **2015**, *27*, 7662–7672.

[39] Fabbri, E.; Nachtegaal, M.; Binninger, T.; Cheng, X.; Kim, B. J.; Durst, J.; Bozza, F.; Graule, T.; Schäublin, R.; Wiles, L. et al. Dynamic surface self-reconstruction is the key of highly active perovskite nano-electrocatalysts for water splitting. *Nat. Mater.* **2017**, *16*, 925–931.

[40] Chen, P. Z.; Tong, Y.; Wu, C. Z.; Xie, Y. Surface/interfacial engineering of inorganic low-dimensional electrode materials for electrocatalysis. *Acc. Chem. Res.* **2018**, *51*, 2857–2866.

[41] Jin, S. Are metal chalcogenides, nitrides, and phosphides oxygen evolution catalysts or bifunctional catalysts? *ACS Energy Lett.* **2017**, *2*, 1937–1938.

[42] Xu, K.; Cheng, H.; Liu, L. Q.; Lv, H. F.; Wu, X. J.; Wu, C. Z.; Xie, Y. Promoting active species generation by electrochemical activation in alkaline media for efficient electrocatalytic oxygen evolution in neutral media. *Nano Lett.* **2016**, *17*, 578–583.

[43] Chen, P. Z.; Xu, K.; Fang, Z. W.; Tong, Y.; Wu, J. C.; Lu, X. L.; Peng, X.; Ding, H.; Wu, C. Z.; Xie, Y. Metallic Co_4N porous nanowire arrays activated by surface oxidation as electrocatalysts for the oxygen evolution reaction. *Angew. Chem., Int. Ed.* **2016**, *54*, 14710–14714.